

This is the author's accepted manuscript. The version of record was published in International Journal of Industrial and Systems Engineering, 2020 Vol. 34 No. 3, pp. 283 – 300, and can be accessed at <https://doi.org/10.1504/IJISE.2020.105739>

Incompressible flows in channels with fluid/porous regions

P.V. Bulat¹, K.N. Volkov²

¹ITMO University, St Petersburg, 197101, Russia

²Kingston University, London, SW15 3DW, United Kingdom

Abstract

Flows in channels with fluid and porous regions important to various engineering applications. A better understanding of fundamental mechanisms in the fluid flows in porous regions are needed to optimize gas bearings, air filters, thermal insulation in the specific applications. Darcy–Brinkman–Forchheimer model is used to describe the flow inside the porous domain. The finite volume method is applied to solve these equations in a porous and open domains. The capabilities of the mathematical model and computational algorithm are demonstrated using test cases from various areas of practical applications. The results of the numerical simulation of flows in porous domains are presented.

Keywords

Porous medium, Computational fluid dynamics, Channel flow, Fluid injection, Gas bearing

1 Introduction

Flows and heat transfer in channels containing both fluid and porous regions are important in many engineering applications (rotor aerodynamics, thrust air bearings, thermal insulation, diesel particulate filters, drinking water treatment) and natural phenomena (filtration process). A better understanding of fundamental mechanisms in the fluid flow and thermal transport are required to optimize the design considerations for various specific applications [1, 2].

The porous body approximation used instead of repetitive structures is one of the approaches to reduce requirements to the computational resources [3, 4]. For a certain type of porous domains, dense-packed spheres, there are valid mathematical expressions for the calculation of resistance factors [5].

A way to improve the reliability and life cycle of rotating machines is the usage of various designs of contactless supports [6, 7]. The bearings which are characterized by a self-contained lubricating mechanism have a stationary porous bushing whose inner diameter faces the bearing clearance, while the outer one faces a wrap-around reservoir.

Laminar flow in a porous channel with variable wall suction, wall injection and variable radial mass flux are investigated in [8, 9] based on coupled solution of Navier–Stokes and Darcy law equations. The forced convection in channels partially filled with porous media is numerically investigated in [10] using Darcy–Brinkman–Forchheimer model. Fluid flow and heat transfer in a channel partially filled with porous medium is analysed in [11]. Analytical and numerical studies of the laminar flow in a porous channel with large suction along the permeable walls and a weakly oscillatory pressure performed in [12]. Friction and heat transfer for fully laminar flow in isothermal parallel plate channel completely filled with porous media are studied in [13]. Darcy equation representing the porous wall conditions is exploited in [14] to simulate fluid flow through a channel with porous walls based on finite element method. The results of finite-difference simulation of a laminar incompressible and isothermal flow in a cylindrical channel with permeable walls are presented in [15].

The interface conditions imposed at the intersection of the fluid and porous sub-domains including gradient reconstruction at the interface or the treatment the advecting and advected velocities at the interface are important for practical applications. Many previous studies have focused on low-Reynolds number flows, where the change in pressure as a result of the change in the advected velocity is negligible. Implementation of the interface conditions into a CFD code [16, 17].

The SIMPLE algorithm of the predictor–corrector type has been adapted to solve Brinkman–Forchheimer equations [3]. A coupled computational algorithm for modified Navier–Stokes equations to simulate flows in anisotropic porous media [18]. The results of numerical simulation of a wide number of injection-driven flows in plane and cylindrical channels are presented in [19, 20].

We use the mathematical model based on Darcy–Brinkman–Forchheimer equations to describe the flow in coupled open and porous domains. Numerical solution of the governing equations is based on the finite volume method and coupled SIMPLE algorithm. The effect of various physical quantities on velocity and pressure distributions is investigated, and the results of the numerical simulation of flows in porous domains are presented. The results obtained are compared with the available data.

2 Methods

2.1 Governing equations

Brinkman–Forchheimer equations of the momentum conservation and continuity describing the laminar steady viscous flow of incompressible fluid in a porous medium, which are written relative to a real velocity, have the form [2]

$$\nabla \cdot (\varepsilon \rho \mathbf{v}) = 0; \quad (1)$$

$$\nabla \cdot (\varepsilon \rho \mathbf{v} \otimes \mathbf{v}) = -\varepsilon \nabla \cdot (p \mathbf{I}) + \nabla \cdot (\varepsilon \boldsymbol{\tau}) - \left(\frac{\varepsilon^2 \mu}{\mathbf{K}} + \varepsilon^3 F \mathbf{C} |\mathbf{v}| \right) \cdot \mathbf{v}. \quad (2)$$

Here, ε is the porosity, ρ is the density of the material to be simulated, \mathbf{v} is the real velocity, p is the static pressure, μ is the dynamic viscosity, F is Forchheimer coefficient depending on the flow parameters, \mathbf{K} is the permeability tensor, \mathbf{C} is the inertial resistance tensor, \mathbf{I} is the unit tensor. The viscous stress tensor for incompressible Newtonian medium is

$$\boldsymbol{\tau} = \mu_B (\nabla \mathbf{v} + \nabla \mathbf{v}^*),$$

where μ_B is the modified Brinkman molecular viscosity in a porous medium. The modified Brinkman molecular viscosity is set in a porous medium. It depends on the medium porosity factor and is represented in the following form [21]

$$\mu_B = (1 - \varepsilon)^{-0.25}.$$

Superscript * corresponds to the conjugate tensor.

The density in equations (1) and (2) remains constant. In general, the porosity coefficient is a function of Cartesian coordinates and time, and does not depend on velocity and pressure. Therefore, the equation of state is not required. The diagonal components of the inertial resistance tensor in isotropic porous media are proportional to $\rho K^{-1/2}$, where K is the permeability. In anisotropic porous media this dependence is invalid, and calculations of the components of the inertial stress tensor are required to take into account sizes of pores and inter-pore spaces, flow regime [22]. The effect of non-linear Forchheimer coefficient is

noticeable at local Darcy numbers above 10^{-3} , so these terms may be neglected only in some cases of a laminar flow [23].

The last two terms in the momentum equation (2) are the Darcy and Forchheimer ones. In real calculations with the use of experimental data on pressure losses it is easy to represent these terms in the form of the resistance tensor

$$P = \frac{\varepsilon^2 \mu}{\mathbf{K}} + \varepsilon^3 FC |\mathbf{v}| = \boldsymbol{\alpha} |\mathbf{v}| + \boldsymbol{\beta},$$

where $\boldsymbol{\alpha}$ is the inertial (non-linear) resistance tensor, $\boldsymbol{\beta}$ is the viscous (linear) resistance tensor. These tensors have a symmetric structure, and in case of the coordinate system coinciding with the main axes of porous medium (axes should be orthogonal) these tensors are diagonal.

2.2 Numerical procedure

Continuity equation (1) and momentum conservation equation (2) describe flows of viscous compressible and incompressible fluids both in porous and open domains, as well as at an interface of different porous media. These equations are also used to solve problems with a porosity ratio varying in space and time.

Discretization of the governing equations is carried out for unstructured meshes with arbitrary cell topology using a cell-centred finite-volume method [18]. The difference from the classic SIMPLE algorithm is in the completely implicit relationship between velocity and pressure owing to the implicit terms of the pressure and mass flow gradients in the continuity equation and momentum equation. One of the attractive features of this algorithm is the possibility of completely implicit discretization of off-diagonal components of the porous medium resistance tensor in the right-hand side of the momentum equation. Implicit discretization allows reducing the number of linear iterations as compared to the SIMPLE algorithm with explicit discretization of off-diagonal components. Linearization is performed with the simple iteration method. The multigrid method is used to solve the system of finite difference equations [24, 25].

3 Channel flows

3.1 Flow in a channel with porous insert

The plane flow through a parallel plane channel with porous plug inserted at some distance from the inlet is considered. The problem is identical to [26] and is shown in the Figure 1, where the shaded region indicates the porous sub-domain. A rectangular insert of length L_2 made of a homogeneous isotropic porous material is placed in the channel at a distance of L_1 to the channel inlet. The channel length L_3 has been chosen sufficiently large to eliminate the impact of steady state flow regions on the final results. The lengths of fluid and porous sub-domains are $L_1=5H$, $L_2=5H$ and $L_3=50H$, where H is the channel height. The large value of L_3 is chosen to ensure fully developed flow at the outlet.

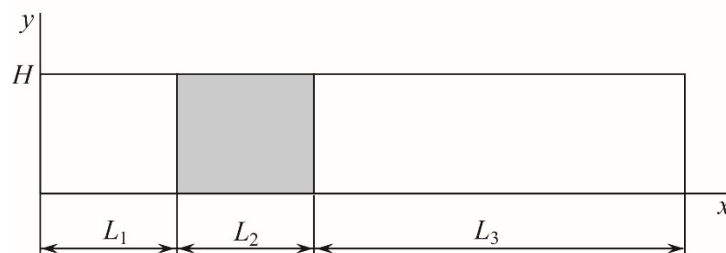


Figure 1. Flow in a channel with porous insert

Two-dimensional problem formulation is considered, and the channel length is eliminated from the consideration by imposing the periodical boundary conditions. The velocity boundary conditions consist of a fully developed plane channel flow specified at the inlet boundary ($x=0$), fully developed conditions at the outlet boundary ($x=60H$) and no-slip and no-penetration conditions at the channel walls ($y=0$ and $y=H$). The pressure is specified as zero at the outlet boundary to set the pressure level, while pressure is extrapolated to all other boundaries. The dimensionless parameters of the problem are Reynolds number, $Re=\rho UH/\mu$, and Darcy number, Da . These numbers are used to select dimensional quantities such as fluid properties and resistance factors for the porous body. The porosity factor ε is set equal to 1.

The flow is simulated for $Re=10^3$ and $Da=10^{-2}$. The tetrahedral mesh containing $\sim 10^5$ cells in porous region is used. Typical streamwise size of the mesh is 0.005 m. The case is solved using a single large time step with a non-linear residual tolerance, normalized by the average magnitude of the given field, specified as 10^{-6} . The computational cost of the coupled algorithm is ~ 25 . The computational cost is measured as a number of steps required to reach the specified level of residual.

The examination of results includes the comparison of velocity and pressure profiles along the centerline of channel. Streamwise velocity and static pressure distributions along the line $y/H=0.5$ are presented on Figure 2 (solid lines). The results computed are compared with [9] (bullets). The results are very similar, although the profiles near the interfaces are slightly different due to different treatment of pressure at interface.

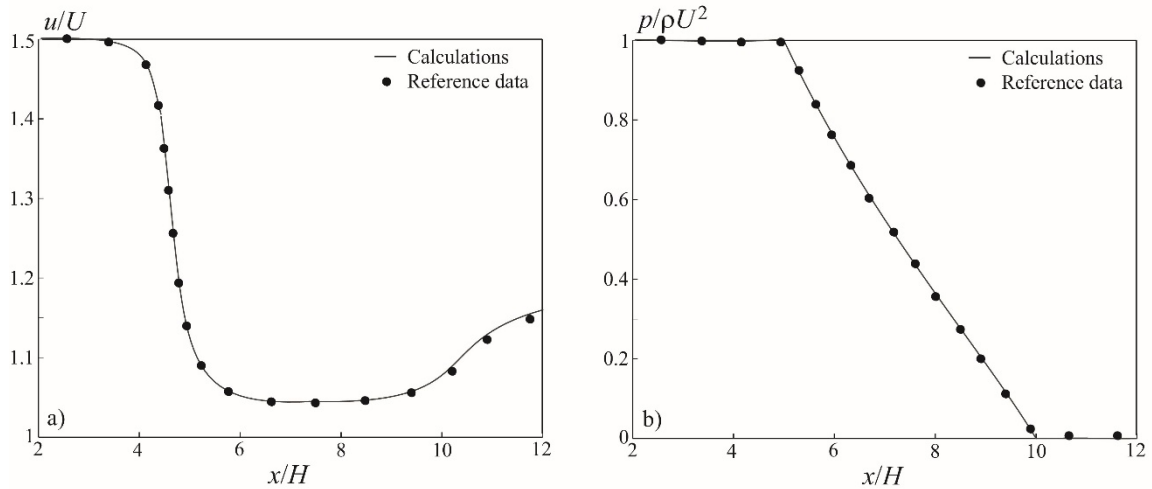


Figure 2. Streamwise velocity (a) and pressure (b) distributions along the line $y/H=0.5$

Results for different Darcy numbers and fixed Reynolds number ($Re=1000$) demonstrate the robustness of model over a wide range of input parameters shown on Figure 3. The model is capable obtaining physically reasonable results for porous materials with low permeability.

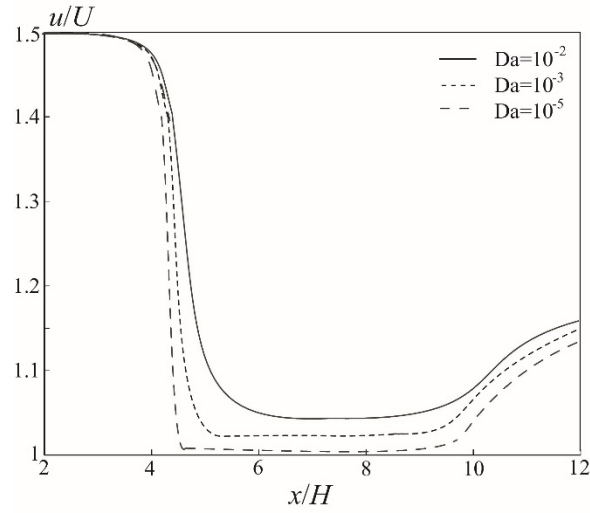


Figure 3. Streamwise velocity distributions along line $y/H=0.5$ at $Re=1000$ and different Darcy numbers

3.3. Flow in a channel with fluid injection through porous walls

Fluid flow in plane and cylindrical channels with fluid injection through porous walls is considered. The fluid and porous domains shown on Figure 4. The flow is assumed to be a fully developed at the inlet of channel with porous walls. On the inner surface of the porous tube, the injection velocity is found from Darcy equation $v_w = -(k/\mu)\text{grad } p$, where k is the porous walls permeability, μ is the dynamic viscosity. If the external pressure p_a is uniform along the centerline and equal to atmospheric pressure, the injection velocity at the wall is found from $v_w = k(p - p_a)/(\mu h)$, where h is the channel wall thickness. The effect of the velocity slip is practically negligible at the inner surface of porous tube [27].

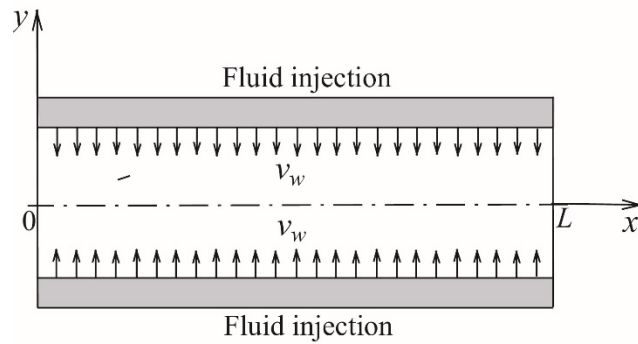


Figure 4. Flow in a channel with fluid injection through porous walls

The fluid used for simulation is the air $\rho=1.21 \text{ kg/m}^3$, $\mu=1.71 \times 10^{-5} \text{ Pa s}$. The porous wall is made of the compacted exfoliated clay, whose its permeability is equal to $1.85 \times 10^{-17} \text{ m}^2$. The computational mesh consists of 400 nodes in the axial direction, and 100 nodes in the radial direction. The mesh nodes are clustered near the injection surface to resolve the vortical wave structure and turbulent boundary layer. The flow structure depend on Reynolds numbers based on inlet velocity and injection velocity

$$\text{Re} = \frac{\rho U_0 H}{\mu}, \quad \text{Re}_w = \frac{\rho V_{w0} H}{\mu},$$

where H is half width or radius of the channel, U_0 is inlet mean velocity. Injection velocity is found as $V_{w0} = k(p_0 - p_a)/(\mu h)$.

At high Reynolds numbers, the flow region in the channel with wall injection is divided into sub-region of influence of viscosity near the walls and sub-region of vortical flow in the core (Figure 5). The njection ($Re_w \rightarrow \infty$) means that the injection velocity considerably, by the order of magnitude, exceeds the velocity in the boundary layer near the impermeable surface, and the injection velocity is considerable lower than the average flow velocity in the channel. In such conditions, the flow in the injected fluid layer turns out inviscid, and the boundary layer is pushed away from the surface and transformed into the mixing layer between the injected layer and the flow in the channel. The thickness of this layer turned out to be small compared to the thickness of the layer of the injected fluid. The streamwise velocity profile for weak injection ($Re_w \rightarrow 0$) is very similar to the velocity distribution in Hagen–Poiseuille flow [28]. Radial velocity profiles are very similar with cases of weak and strong injection (Figure 6).

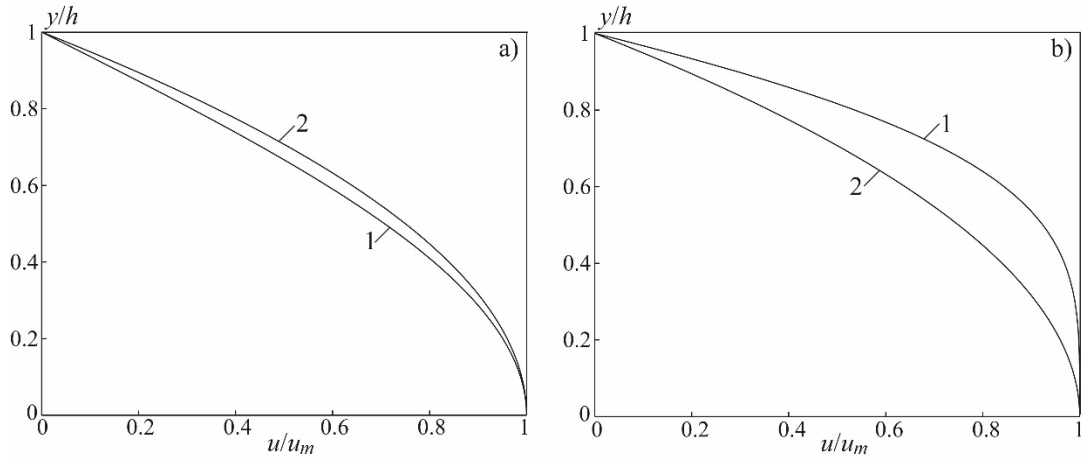


Figure 5. Streamwise velocity profiles in planar (a) and cylindrical (b) channels with weak (lines 1) and strong (lines 2) injection

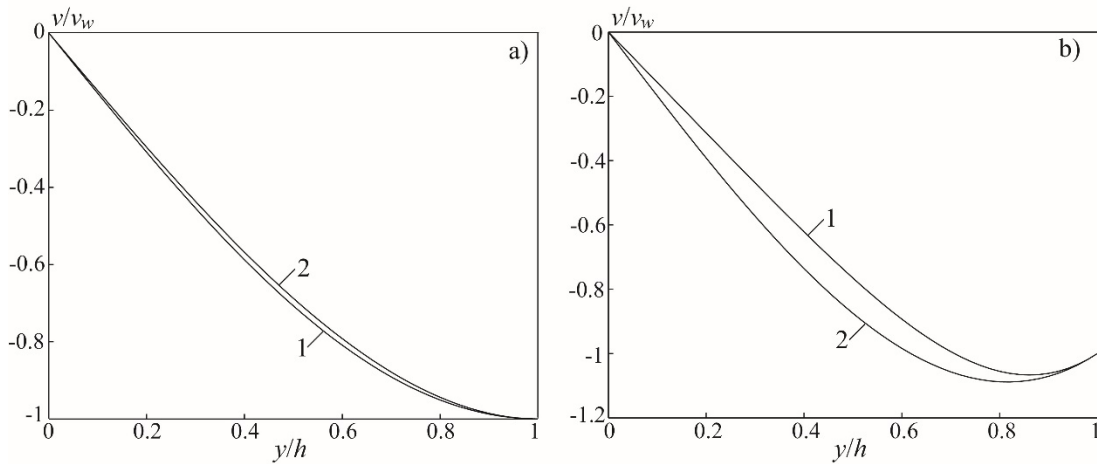


Figure 6. Radial velocity profiles in planar (a) and cylindrical (b) channels with weak (lines 1) and strong (lines 2) injection

4 Power output of wind turbine

Actuator disc model is used as a simple method for simulating horizontal axis tidal turbines. Actuator disc produces a similar far wake to a real turbine, but eliminates some of the scaling issues which occur in experiments, and reduces the mesh resolution required in CFD simulations. The porous loss model takes into account the pressure gradient, $\Delta p/l$, through the porous region using a user-defined quadratic loss coefficient, K . The material is defined as having a drag coefficient, k , which relates the pressure drop across the disc with the velocity

at the disc location. The resistance coefficient of the turbine to the flow is introduced as follows

$$k = \frac{2(p_1 - p_2)}{\rho u^2},$$

where p_1 and p_2 are the static pressures immediately upstream and downstream of the rotor, respectively, u is the one-dimensional wind speed immediately upstream of the rotor, and ρ is the air density. This equation gives output power as function of resistance coefficient

$$P = \eta_t (p_1 - p_2) u A = \frac{1}{2} \eta_t k \rho u^3 A,$$

where η_t is the efficiency of the turbine, and A is the flow area.

Disc porosity, which is represented by their quadratic resistance coefficient, K , varies to embrace a range of simulated disc resistance which goes from 0 (which is equivalent to a solid wall) up to 8 kg/m^4 . This approach allows finding the point of maximum power output from the actuator disc. In fact, power output would increase from $K=0$ up to a certain value and then, it experiences and steady decreases.

Calculation of pressure drop must be done based on a chosen reference velocity. There are two options for this. The first one is the superficial velocity, which is the velocity which would exist if the porosity $K=1$, and the second option is the true velocity, which is the actual velocity in the porous region flow passages. The superficial velocity is used in this study.

A single porous disc simulating a wind turbine is placed (Figure 7). The chosen diameter of the disc is 46 m. A centre point of the disc is located in the vertical of maximum clear height. Distance from ground to the centre point is 29 m. The distance of the lowest point of the disc to the terrain is fixed at 6 m, while the separation from the highest point of the turbine to the upper boundary is 8.62 m. The swept area of the disc comprises 1661.9 m^2 and length of the porous disc is set to 3 m long, which is enough to simulate the blades influence.

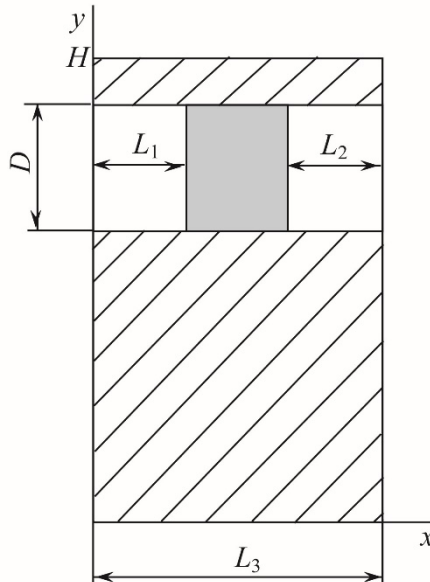


Figure 7. A building structure with an integrated duct containing a porous region

The power law is developed empirically to represent wind shear. The wind height variation is calculated as follows

$$\frac{u}{u_a} = \left(\frac{y}{y_a} \right)^\beta,$$

where u is the averaged wind speed at height y , u_a is the averaged wind speed at height y_a . The power law exponent is a function of wind speed and surface roughness length (type of terrain), and it varies for different types of terrain. The surface roughness length varies according to the terrain of the site. The chosen roughness length is fixed at 0.1 m.

Two domains have been included, porous domain and fluid domain. The first domain is formed by the porous discs which simulate the wind turbine rotors, while the second domain simulates the air flow surrounding the rotors, the viaduct and the ground. The method represents the swept volume of the wind turbine blades as a porous medium, and by adjusting the resistance of the porous medium the balance between the energy extraction and the bypass flow can be optimized.

To simulate the porous plug resistance, the solution set up needs to be changed by editing the porous domain settings. To do this, the porous plug domain is given certain porosity. This is a value between 0 and 1 which represents the available open flow area. The value of 0.9 means that the porous medium creates a 10% reduction in flow area or a 10% increase in local flow velocity. This reduction in flow area can be thought of as representing the flow area which would be occupied by the actual blades and hub of a wind turbine rotor.

The quadratic residence coefficient varies from 0 to 8 kg/m⁴ to simulate different types of rotor characteristics regarding to its absorption of wind power by means of a pressure drop. The calculations are launched on unstructured meshes containing about 2 millions of cells.

Dependence of the power output on quadratic resistance coefficient is shown in the Figure 9. The power output is around 16000 W for $K=0.1$ kg/m⁴ and it is increased up to 27269 W, which represents 70% more. At this point, the power starts a stable progression with a peak of power on $K=0.5$ kg/m⁴ with $P=29129$ W. Then, it slightly decreases with small changes for $K=0.7$ kg/m⁴ and 0.9 kg/m⁴, where there is a decrease of 0.4% and 2.6% respectively, respecting to the peak point. From this situation, the power extraction from the porous disc decreases steadily. However, there is a sudden low for $K=1.1$ kg/m⁴, where power decreases by 27% and then it is increased by 25%. Despite this simulation is repeatedly carried, the result remains in the same figures. This result would likely be due to simulation issues (using higher calculation potency this result would not appear). Regarding to the last K value ($K=8$ kg/m⁴), the power production would be 14795 W.

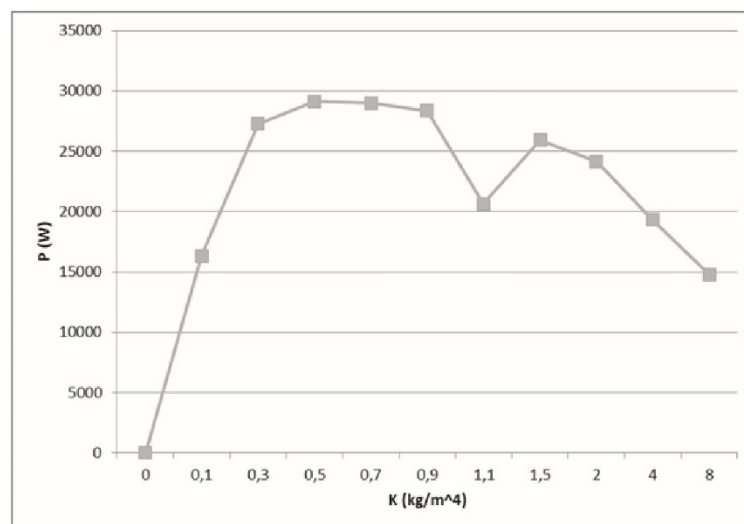


Figure 9. Power output of a wind turbine as a function of resistance coefficient

6 Conclusion

A numerical model was developed for analysis of the fluid flows in conjugate fluid and porous domains using unstructured meshes. The coupled computational algorithm for Brinkman–Forchheimer equations to simulate flows in anisotropic porous media is applied. In contrast to the SIMPLE algorithm, the coupled algorithm couples the velocity and pressure in the algebraic form in a completely implicit manner. Coupling is performed owing to the implicit pressure gradient and mass flux terms in the momentum and continuity equations, respectively. The robustness of the developed numerical methods was demonstrated for some simple benchmark flow cases through a porous media. Verification and validation of the CFD solver has been made for some benchmark cases including fluid flow through a porous material insert, a fluid flow in a planar divided channel and a fluid flow through a channel with porous walls.

The results obtained are potentially beneficial for design and optimization of the porous bearings. They have some advantages against classic solid hydrodynamic bearings including the elimination of a circulatory system for lubricant, the reduction in load carrying capability, the reduction in stability due to higher attitude angles, the capability to run at higher speeds without overheating due to the reduced shear in the clearance region.

Acknowledgements

This work was financially supported by the Ministry of Education and Science of Russian Federation (agreement No 14.578.21.0203, unique identifier of applied scientific research RFMEFI57816X0203).

References

1. Kaviany M. Principles of heat transfer in porous media. New York: Springer-Verlag, 1991, 626 p.
2. Nield D.A., Bejan A. Convection in porous media. New York: Springer Science, 2013, 778 p.
3. Costa V.F., Oliveira L.A., Baliga B.R., Sousa A.C.M. Simulation of coupled flows in adjacent porous and open domains using a control-volume finite-element method. Numerical Heat Transfer, 2004, 45, 675–697.
4. Ozden E., Tari I. Shell side CFD analysis of a small shell-and-tube heat exchanger. Energy Conversion and Management, 2010, 51, 1004–1014.
5. Ergun S. Fluid flow through packed columns. Chemical Engineering Progress, 1952, 48(2), 89–94.
6. Bulat M.P., Bulat P.V. Basic classification of the gas-lubricated bearing. World Applied Sciences Journal, 2013, 28(10), 1444–1448.
7. Beschastnyh V.N., Bulat P.V. Method of sliding bearings static characteristics calculation. American Journal of Applied Sciences, 2014, 11(11), 1959–1963.
8. Galowin L.S., Fletcher L.S., De Santis M.J. Investigation of laminar flow in a porous pipe with variable wall suction. AIAA Journal, 1974, 12, 1585–1589.
9. Belfort G. Fluid mechanics in membrane filtration: recent developments. Journal of Membrane Science, 1989, 40, 123–147.
10. Jang J.Y., Chen J.L. Forced convection in a parallel plate channel partially filled with a high porosity medium. International Communications in Heat Mass Transfer, 1992, 19(2), 263–273.

11. Jen T.-C., Yan T.Z. Developing fluid flow and heat transfer in a channel partially filled with porous medium. *International Journal of Heat and Mass Transfer*, 2005, 48, 3995–4009.
12. Jankowski T.A., Majdalani J. Laminar flow in a porous channel with large wall suction and a weakly oscillatory pressure. *Physics of Fluids*, 2002, 14(3), 1101–1110.
13. Hamdan M.O. An empirical correlation for isothermal parallel plate channel completely filled with porous media. *Thermal Science*, 2013, 17(4), pp. 1061–1070.
14. Nassehi V. Modelling of combined Navier–Stokes and Darcy flows in crossflow membrane filtration. *Chemical Engineering Science*, 1998, 53, 1253–1265.
15. Damak K., Ayadi A., Zeghmami B., Schmitz P. A new Navier–Stokes and Darcy's law combined model for fluid flow in crossflow filtration tubular membranes. *Desalination*, 2004, 161, 67–77.
16. DeGroot C.T., Straatman A.G. A finite-volume model for fluid flow and nonequilibrium heat transfer in conjugate fluid-porous domains using general unstructured grids. *Numerical Heat Transfer B*, 2011, 60, 252–277.
17. Alazmi B., Vafai K. Analysis of fluid flow and heat transfer interfacial conditions between a porous medium and a fluid layer. *International Journal of Heat and Mass Transfer*, 2002, 44, 1735–1749.
18. Kozelkov A.S., Lashkin S.V., Tsibereva Yu.A., Volkov K.N., Tarasova N.V. An implicit algorithm of solving Navier–Stokes equations to simulate flows in anisotropic porous media. *Computers and Fluids*, 2018, 160, 164–174.
19. Emelyanov V.N., Teterina I.V., Volkov K.N., Garkushev A.U. Pressure oscillations and instability of working processes in the combustion chambers of solid rocket motors. *Acta Astronautica*, 2017, 135, 161–171.
20. Soto Hernandez O., Volkov K., Martin Mederos A.C., Medina Padron J.F., Feijoo Lorenzo A.E. Power output of a wind turbine installed in an already existing viaduct. *Renewable and Sustainable Energy Reviews*, 2015, 48, 287–299.
21. Brinkman H. The viscosity of concentrated suspensions and solutions. *The Journal of Chemical Physics*, 1952, 4(20), 571–584.
22. Muljadi B.P., Blunt M.J., Raeini A.Q., Bijeljic B. The impact of porous media heterogeneity on non-Darcy flow behaviour from pore-scale simulation. *Advances in Water Resources*, 2016, 95, 329–340.
23. Prasad V., Kulacki F.A., Keyhani M. Natural convection in porous media. *Journal of Fluid Mechanics*, 1985, 150, 89–119.
24. Volkov K.N., Kozelkov A.S., Lashkin S.V., Yalozo A.V. A parallel implementation of the algebraic multigrid method for solving problems in dynamics of viscous incompressible fluid. *Computational Mathematics and Mathematical Physics*, 2017, 57(12), 2030–2046.
25. Mavriplis D.J. An assessment of linear versus nonlinear multigrid methods for unstructured mesh solvers. *Journal of Computational Physics*, 2002, 175(1), 302–325.
26. Betchen L.J., Straatman A.G., Thompson B.E. A nonequilibrium finite-volume model for conjugate fluid/porous/solid domains. *Numerical Heat Transfer A*, 2006, 49, 543–565.
27. Schmitz P., Prat M. 3-D laminar stationary flow over a porous surface with suction: description at pore level. *AIChE Journal*, 1995, 41, 2212–2226.
28. Culick F.E.C. The stability of one-dimensional motions in a rocket motor. *Combustion Science and Technology*, 1973, 7(4), 165–175.